DOI: 10.12398/j.issn.2096-7217.2025.02.002

Design and experiment of an automated honey-harvesting robot

ZHANG Di[1], WANG Chunying[1, 2, 3], YANG Mingguo[1], SUN Zixuan[1], LIU Ping[1, 2, 3*]

(1. *College of Mechanical and Electronic Engineering, Shandong Agricultural University, Tai'an* 271000, *China*;
2. *Shandong Engineering Research Center of Agricultural Equipment Intelligentization, Tai'an* 271000, *China*;
3. *Shandong Key Laboratory of Intelligent Production Technology and Equipment for Facility Horticulture, Shandong Agricultural University, Tai'an* 271000, *China*)

Abstract: The conventional honey production is dominated by fragmented, small-scale individual farming models. The traditional approach of honey-harvesting involving manual beehive frames extraction, beeswax layer excision and centrifugal honey separation, expose beekeepers to potential bee stings and frequently compromise honeycomb integrity. To address these limitations, we designed an automated honey-harvesting robot capable of autonomous frame extraction and beeswax removal. The robot mainly consists of a mobile mechanism equipped with image recognition for beehive localization, a magnetic adsorption-based beehive frame handling device (60.8 N maximum suction) coupled with a cross-slide mechanism for precise frame manipulation, and a thermal beeswax layer-melting apparatus, with optimal melting parameters (15 m/s airflow at 90 ℃ for 30 seconds) determined through rigorous thermal flow simulations utilizing FLUENT/Mechanical software. Field experiments demonstrated beehive frames handling success rate exceeding 85%, beeswax layer removal efficacy over 80% and damage of honeycombs below 30%. The experiment results validate the robot's operational reliability and its capacity to automate critical harvesting procedures. This study significantly reduces the labor intensity for beekeepers, effectively eliminates the risk of direct human-bee contact and improves the removal of beeswax layer, thereby catalyzing the modernization of the beekeeping industry.

Keywords: honey-harvesting; automated; beeswax layer-melting; fluid-structure interaction; parameter optimization

CLC number: S225.99　　**Documents code:** A　　**Article ID:** 2096-7217 (2025) 02-0024-11

ZHANG Di, WANG Chunying, YANG Mingguo, SUN Zixuan, LIU Ping. Design and experiment of an automated honey-harvesting robot [J]. Journal of Intelligent Agricultural Mechanization, 2025, 6(2): 24－34
张迪, 王春颖, 杨明国, 孙梓轩, 刘平. 蜂蜜自动化采收机器人的设计与试验[J]. 智能化农业装备学报(中英文), 2025, 6(2): 24－34

0　Introduction

Honey, a primary constituent of apiary products[1], is rich in sugars, water and enzymes, and a diverse array of phytochemicals, possessing significant nutritional and medicinal value[2-3]. An analysis based on six decades of data from the Food and Agriculture Organization of the United Nations (FAO) reveals that honey production has nearly tripled. However, this growth rate lags behind the continually increasing consumer demand[4]. Consequently, there is an urgent need for improving honey harvesting methods to optimize the industrial structure and meet the growing consumer demand[5-6].

Received date: 2024-12-31　　**Revised date:** 2025-02-06

Foundation item: National Natural Science Foundation of China (31700644); Shandong Province Postdoctoral Innovation Project (SDCX-ZG-202400195)

First Author: ZHANG Di, Postgraduate, research interests: intelligent control technology for agricultural equipment. E-mail: 2023120771@sdau.edu.cn

* **Correspondence Author:** LIU Ping, Doctor, Professor, research interests: intelligent control technology for agricultural equipment. E-mail: liuping@sdau.edu.cn

The rapid development of modern agricultural technologies has led to significant changes in the traditional methods of harvesting of agricultural produce[7]. Compared to the agricultural automation equipment for crops, beekeeping, as a niche agricultural industry, has received comparatively limited attention[8]. Given the extensive globle prevalence of beekeeping across numerous regions[9], there is an urgent need to develop automated machinery to modernize the beekeeping industry. However, most automated equipment focuses on the purification and processing of honey[10], with relatively little development on equipment for the harvesting process[11-12]. Contemporary honey harvesting employs smoke to pacify bee aggression, avoiding open flames to safeguard bees and their larvae[13]. The automated machinery for honey harvesting is recognized as an efficacious means of conserving labor and protecting beekeepers[14]. The design of the end-effector, navigation systems and target recognition capabilities are crucial aspects in the development of harvesting robots[15-16].

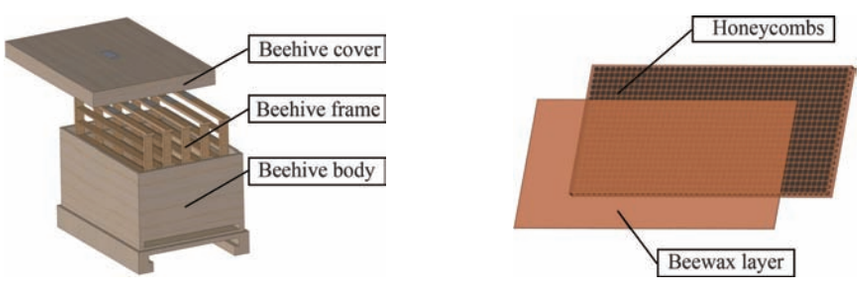
These components are essential for enhancing the operational efficiency and adaptability of robots in complex environments. Meanwhile, the balance between cost and operational accuracy plays a crucial role in robot′s development, exerting a decisive influence on the marketability of the robot. To minimize damage to honeycombs, researchers have proposed numerous methods for beeswax layer removal, including both physical and biological methods[17-18]. While these approaches demonstrate efficiency, their high costs and challenges in integration into automated systems remain significant barriers.

This study introduces an automated honey-harvesting robot designed to eliminate direct human-bee interaction and facilitate unmanned harvesting operations. Furthermore, a novel beeswax removal method employing controlled heating is proposed. Comprehensive numerical simulations, utilizing fluid-structure interaction analysis[19-20], are carried out to optimize the parameters for the melting process. The feasibility of the automated honey-harvesting robot and the reliability of the optimized parameters were subsequently validated through field experiments. This study holds significant practical prospects and value for the modernization and advancement of the beekeeping industry.

1　Materials and methods

1.1　Movable-frame beehive

The design of the movable-frame beehive fully accounts of the behavioral habits of bees, offering exceptional flexibility and ease of management, thereby providing a solid foundation for modern scientific beekeeping[21]. The beehive frame is a structure designed to secure the combs within the beehive[22]. It serves as the core of the movable-frame beehive system. In this study, the widely applicable seven-frame standard beehive for Apis cerana cerana Fabricius was selected as the reference for designing an automated honey-harvesting robot[23], as shown in Figure 1(a).



(a) 3D models of a movable-frame beehive　　(b) 3D models of honeycombs and beeswax layer

Figure 1　Structure of the experimental subject

The dimensions of the beehive are 540 mm×380 mm×370 mm, with individual beehive frames measuring 480 mm ×330 mm. The honeycombs exhibit a typical hexagonal cell structure, overlaid with a thin beeswax layerto protect the honey-filled combs. In this study, SpaceClaim software, was employed to develop models for both honeycombs and beeswax layer, as shown in Figure 1(b). Honeycomb materials, characterized by a tensile strength exceeding their compressive strength, are prone to compressive

collapse. However, excessively thin walls require dense mesh discretization for numerical simulations, consuming significant computational resources. Given that bees demonstrate the ability to repair damaged individual honeycombs, this investigation prioritized the simulation of the overall structural and physical properties rather than the detailed behavior of individual cells. To this end, the model was simplified by increasing the wall thickness and disregarding the specific arrangement of individual hexagonal cells. Meanwhile, a reduced compressive strength was assigned to the honeycomb's material in the simulation. Ultimately, field experiments were conducted to validate the simulation outcomes.

1.2 Design of automated honey-harvesting robot

Based on the parameters of the movable-frame beehive, the study designed an automated honey-harvesting robot, as depicted in Figure 2. It was primarily comprised of these essential components: the mobile mechanism, the beehive frame handling device, an industrial camera, the beeswax layer-melting apparatus and a compact controller. The main parameters of the robot's component are shown in Table 1.

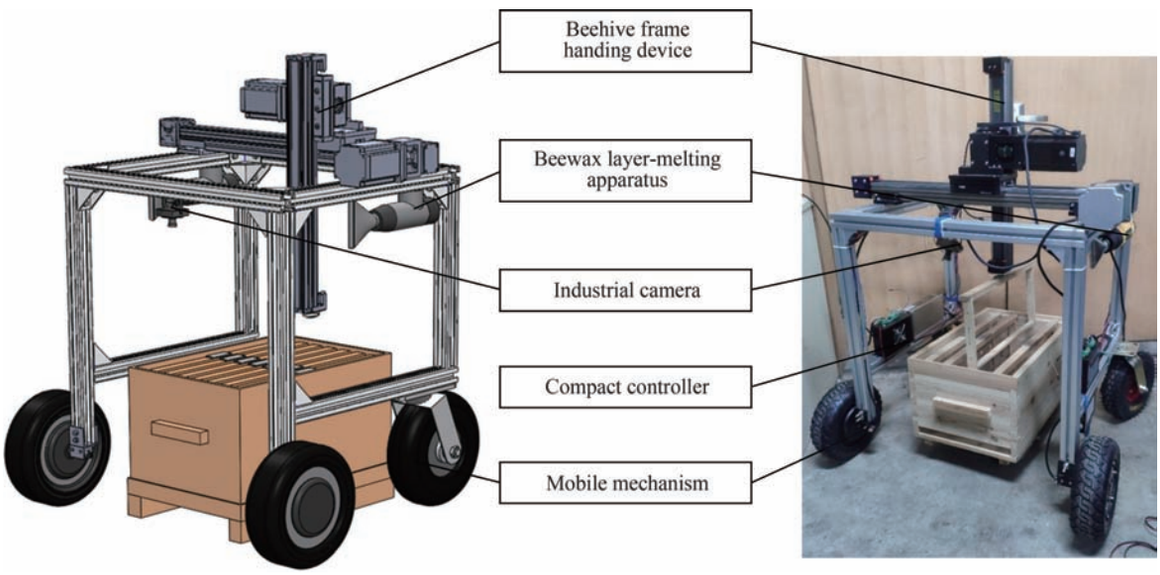


Figure 2 Overall structure of an automated honey-harvesting robot

Table 1 Types and parameters of the automated honey-harvesting robot main components

Component	Types	Parameters
Robot's frame	Aluminum Profile (4040) /(mm×mm×mm)	54×115×60
Hub motor	JBG2210H5B124036D1	Diameter: 10.5 inches, Max load: 120 kg, Power: 350 W, Torque: 13 N·m
Driven wheel	Industrial Caster	Diameter: 10 inches, Max load: 200 kg
Linear actuator	KNK Sync Belt Module	*X*-axis travel: 500 mm, Max load: 20 kg; Z-axis travel: 400 mm, Max load: 25 kg
Electromagnet	ELE-P25/11	Suction force: 5 kg, Diameter: 25 mm, Thickness: 11 mm
Industrial camera	DW800	Pixel size: 1.62 μm × 1.62 μm, Noise level: 39 dB, Dynamic range: 72.5 dB
Industrial hot air blower	Zcanz LK-620E	Size: 240 cm × 70 cm × 210 cm, Temperature: 20 ℃ to 1 150 ℃
Controller	STM32F103RBT6	Core: ARM Cortex M3, Speed: 72 MHz, Memory: 128 KB, PWM: 16 Bits

The workflow of the automated honey-harvesting robot was as follows: The mobile mechanism navigated to the target beehive and adjusted its pose. Subsequently, the beehive frame handling device employed an electromagnet to open the beehive cover and then utilized the same method to extract the beehive frames. The positioning of the electromagnet is controlled by a linear actuator. Prior to the mobile

platform transporting the frames to the centrifugal processing unit, a beeswax melting procedure is executed. Then, the beehive frame handling device precisely positioned the frames within the centrifuge's secured fixture. Following the centrifugal extraction process, the mobile mechanism returned the frames to their original locations in the beehive.

1.2.1　Mobile mechanism

The mobile mechanism was designed with a sturdy four-wheel gantry configuration, constructed from durable metallic materials. Two hub motors were integrated into the front axle, enabling precise control of both linear and curvilinear movements, thereby ensuring the accuracy of navigation by adjusting the speeds of the wheels. Furthermore, the two driven wheels were positioned at the rear, facilitating enhanced rotational maneuverability. To enable real-time determination of the pose of the mobile mechanism for positional and orientational correction, a mathematical model for the harvesting machine was then established in this study, as shown in Figure 3.

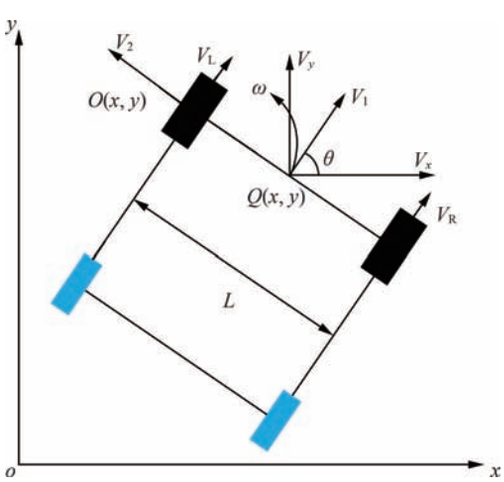


Figure 3　Mathematical model of the mobile mechanism

The direction of the mobile mechanism's head was designated as V_1, while the V_2 direction was determined based on the right-hand rule. In this study, the angular velocities of the two hub motors were set at 10 r/min and 100 r/min, respectively, to induce rotational motion. Given a hub motor diameter of 10.5 inches, the corresponding linear velocities of the left hub motors V_L and right hub motors V_R, were calculated to be 0.14 m/s and 1.37 m/s, respectively. The velocity components of the mechanism could be expressed as Formula 1 and Formula 2[24].

$$\begin{cases} \dfrac{V_L}{R-\dfrac{1}{2}}=\omega \\ \dfrac{V_R}{R+\dfrac{1}{2}}=\omega \end{cases} \tag{1}$$

$$\begin{cases} V_x=\dfrac{1}{2}(V_L+V_R)\sin\theta \\ V_y=\dfrac{1}{2}(V_L+V_R)\cos\theta \end{cases} \tag{2}$$

The above velocity composition formula was derived from the geometric relationships of the mobile mechanism model. The ω signified the angular velocity of the mobile mechanism's center. V_1 and ω could be calculated by Formula 3.

$$\begin{cases} V_1=\dfrac{V_L+V_R}{2} \\ \omega=\dfrac{V_R-V_L}{L} \end{cases} \tag{3}$$

where L was 1.85 m, which represented the axle distance between the hub motors. The radius of rotation R, which was obtained when the mobile mechanism performed a differential turn with point O as the center, could be estimated as V_1 divided by ω and it was calculated to be 1.13 m. If the pose of the mobile mechanism at the initial moment was $Q_0=[X_0, Y_0, Z_0]^T$, its pose at time t was given by Formula 4.

$$Q=[X_t, Y_t, Z_t]^T=\begin{bmatrix} X_0+\int_0^t V_x\mathrm{d}T \\ Y_0+\int_0^t V_y\mathrm{d}T \\ \theta_0+\int_0^t \omega\mathrm{d}T \end{bmatrix} \tag{4}$$

The mobile mechanism relied on hub motors to execute movement commands, with encoders providing real-time feedback on motor operation. The controller ensured that the hub motors operated as preset, dynamically adjusting the harvesting apparatus position and trajectory based on feedback of speed and position.

After the mobile mechanism arrived at the target location along the preset route, an industrial-grade camera took images of the area below the robot. The controller subsequently converted these images to binary format and applied thresholds to identify the beehive's edge features, allowing for fine-tuning of the

robot's position and orientation. In this study, the first-order derivatives and the roberts operator were employed for image gradients computation[25-26]. The controller directed the mobile mechanism to the target point, then identified the edges of the beehive, as shown in Figure 4. The pixel count within the area of the beehive cover in the images captured by the industrial camera was quantified. The image was acquired at a resolution of 1 280 pixels × 960 pixels to optimize the balance between image clarity and computational efficiency. An MJPG frame rate of 30 fps was implemented to satisfy the dynamic adjustment requirements of the mobile mechanism. Empirical testing revealed that the nominal pixel count within the beehive cover area was 1.62×10^5 pixels. Deviations from this target value triggered the control system to activate the hub motors, thereby adjusting the pose of the automated honey-harvesting robot.

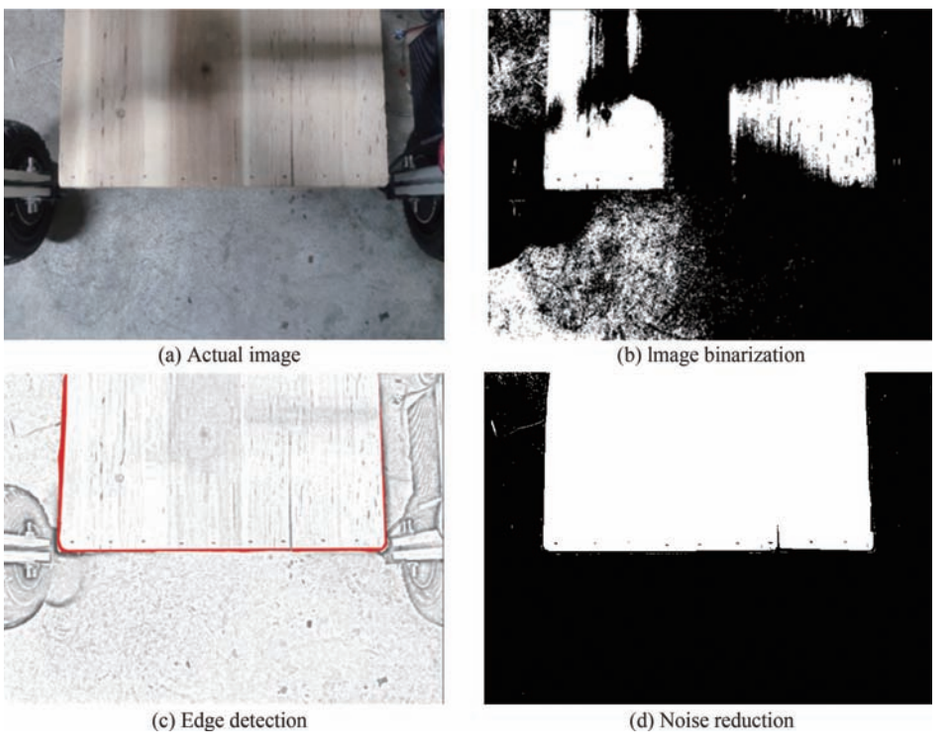


Figure 4 Edge detection process for the beehive

For example, an actual detection results shown in Figure 4, the pixel count within the area of a beehive was 2.48×10^5 pixels, exceeding the established standard. Consequently, a corresponding backward displacement of the mobile platform was required.

1.2.2 Beehive frame handling device

Traditional manual honey harvesting procedures necessitate human intervention for beehive cover removal and frame extraction. However, the beehive frame handling device facilitates the automation of these tasks by employing the controllable magnetic force of an electromagnet to attract ferrous pieces. Thin ferrous pieces were installed on the beehive cover and each beehive frame at strategically selected positions, specifically at the center of gravity directly above, to ensure stability. This study analyzed the force applied to the beehive cover and beehive frames for the selection of an appropriate electromagnet-ferrous piece combination, as given in Formula 5.

$$F_T = G + F_A \tag{5}$$

where the electromagnet's required suction force (F_T) was affected by the gravity (G) on the beehive frames and cover, and the adhesion force (F_A) between them. When the distance between the electromagnet and the ferrous piece was 0, F_T was related to the magnetic flux density B_p and the cross-sectional area S, as given in Formula 6.

$$F_T = \left(\frac{B_p}{4\,965}\right)^2 \times S \times g \tag{6}$$

where the conversion constant for magnetic flux density B_p in Gauss was 4 965. The electromagnet selected for this study had a diameter of 25 mm and the cross-sectional area S was about 490 mm^2. The g denoted the

gravitational acceleration was 9.8 m/s^2. Firstly, the gravity force on the beehive cover was measured to be 44.1 N. Table 2 shows the gravity force on the beehive frames and the adhesion force between a beehive cover and beehive frames.

Table 2　Mechanical properties of movable-frame beehives with varying honey amounts

Different amounts of honey/%	Gravity force on beehive frames/N	Adhesion Force/N	Minimum suction/N
0	14.21	1.20	45.30
25	19.11	1.55	45.65
50	24.79	2.03	46.13
75	30.79	2.78	46.88
100	34.40	3.60	47.70

Furthermore, this study measured the gravity force on the beehive cover to be 44.1 N. After performing calculations, it was determined that a minimum suction force of 47.7 N is required. The ferrous piece assembly that works with the electromagnet is 60 mm × 27 mm × 3 mm in size. After conducting tests, the electromagnet-ferrous piece combination could generate a maximum magnetic force of 60.8 N.

The Beehive frame handling device employs the linear actuator to precisely govern the displacement of the electromagnet. To facilitate the operational manipulation of beehive frames, the vertical rail necessitates a minimum extension of 240 mm, ensuring complete extraction from the movable-frame beehive. Furthermore, the horizontal rail must possess a travel distance greater than the beehive's overall width, with a minimum of 350 mm. The controller is configured to identify the ferrous pieces based on the images transmitted from the industrial camera. Subsequently, utilizing the positional data of the ferrous pieces, the controller directs the linear actuator to execute precise positioning of the beehive cover and beehive frames. Upon attainment of the positioning process, the magnetic suction apparatus is promptly activated for the operation of the opening of the beehive covers and the extracting of beehive frames.

1.2.3　Beeswax layer-melting apparatus

The localized bee repellent and beeswax-melting functionality were achieved through the beeswax layer-melting apparatus based on the industrial hot air blower Zcanz LK-620E. When the apparatus was activated, the blower directed air into the heater, where the air stream was heated by the heating element. An airflow adjuster enabled precise regulation of the air volume and working temperature, as described in Formula 7.

$$Q = V \times \Delta t \times K \tag{7}$$

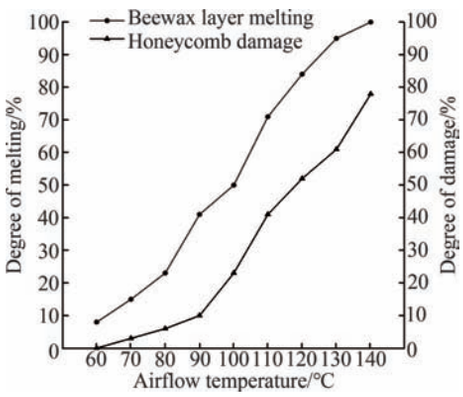
Where the Q denoted the heat energy (J) and the V was 3.6×10^{-2} m^3, which denoted the total volume of the heating space. The Δt denoted the temperature difference from outdoor temperature (27 ℃). The K was 2.67×10^{-2} W/(m·℃), in this study, which denoted the thermal insulation coefficient. Due to variable honey saturation in the beehive, the wax presented the heterogeneous distribution across the honeycomb surface. An excessively broad heating area could result in non-uniform thermal gradients. Specifically, prolonged exposure to elevated pressure and temperature could damage the honeycomb structure in unsaturated areas. Conversely, insufficient heating in honey-saturated areas could result in incomplete beeswax liquefaction. Therefore, based on the main parameters of the hot air blower, the optimal air pressure for the device was calculated using Formula 8 in this study.

$$W_p = 0.5 \times r_0 \times v^2 \tag{8}$$

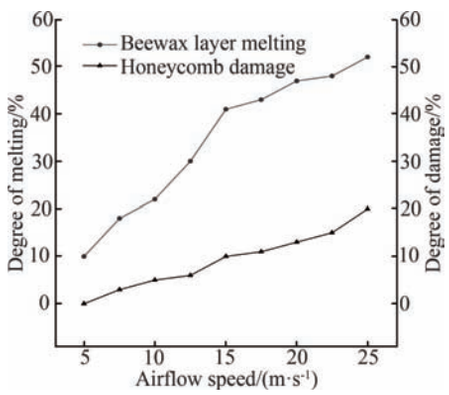
where the W_p denoted the wind pressure and the v was the airflow speed. The 0.5 represented the coefficient for the distribution of kinetic energy in fluids. The r_0 was 1.29 kg/m^3, which represented the Density of air. After calculations, the W_p was 145 N/m^2 at a standard wind speed of 15 m/s under the condition of room temperature.

To determine the best position for the apparatus's air outlet, this study selected six beehive frames of identical size and similar shape, dividing them into two groups of three. The industrial hot air blower was placed above and directly in front of the beehive frames, at distances of 0.1 m, 0.2 m, and 0.3 m respectively. Under ambient temperature conditions of 17 ℃, the blower was activated at a standard airflow velocity of 15 m/s for 10 seconds. Both the efficacy of bee repulsion and the degree of beeswax layer liquefaction were observed in all six experiments. The optimal air outlet position was determined to be at a horizontal distance of 0.2 m directly facing the side of the beehive frame. In

addition, this study conducted single-variable experiments to preliminarily determine the range of melting temperature and airflow speeds, as illustrated in Figure 5.



(a) Beeswax layer melting and honeycomb damage with temperature



(b) Beeswax layer melting and honeycomb damage with airflow speed

Figure 5 Single-variable experiments for temperature and airflow speed

Within the temperature range of approximately 80 ℃ to 100 ℃, the beeswax layer was melted effectively and the damage to the honeycomb remained below 25%, Therefore, this temperature range was deemed reasonable for striking a balance between the beeswax layer melting and minimizing honeycomb damage. Similarly, a reasonable range for the airflow speed was approximately 10 m/s to 25 m/s.

1.3 The numerical simulation methodology

To determine the optimal parameters of the beeswax layer-melting apparatus, computational fluid dynamics (CFD) modeling was essential. This study employed the ANSYS software for fluid-structure interaction simulation analysis to achieve this objective. In the FLUENT software, a simulation of the unidirectional airflow produced by an industrial hot air blower was conducted. A sufficiently large airflow field established for the analysis, as shown in Figure 6. The transient analysis was set up, with the gravitational acceleration configured to -9.8 m/s^2 in the positive Y-axis direction. Additionally, both the energy equation and the K-omega viscous model were activated. Based on the preceding experimental data, reasonable boundary conditions were set, with the airflow field initialized to the outdoor temperature of 27 ℃.

In Workbench workflow, a static structure of the honeycombs and beeswax layer were created for the fluid-structure interaction simulation. The engineering data for the honeycomb was selected as epoxy resin[27-29]. Based on the epoxy resin material, the material density, Poisson's ratio and elastic modulus were fine-tuned. The material was adjusted to 1 100 kg/m^3, with a Poisson's ratio set to 0.2 and a Young's modulus set to 1 GPa. Other mechanical properties were then determined using these values as a basis. The solution results from the FLUENT software were imported into the created static structure, with the pressure and body temperature being introduced as loads into the Mechanical software. Subsequently, the changes in the physical properties of the honeycombs and beeswax layer were calculated and analyzed.

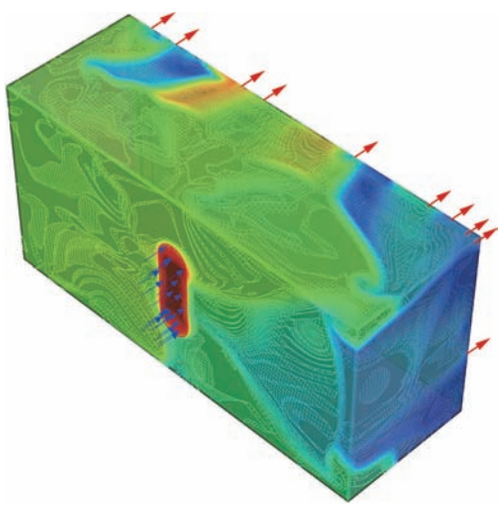


Figure 6 The airflow field contour map

2 Result and discussion

2.1 The simulation and optimization of the beeswax layer-melting apparatus

A larger deformation indicated more effective melting of the beeswax layer, while it also led to greater damage to the honeycombs. To quantitatively assess

the individual impacts of temperature and airflow speed on overall structural deformation, a series of single-variable numerical simulations were executed. The heating time could be precisely controlled by power cycling, while temperature and wind pressure regulation proved more challenging due to the complex control mechanisms of the heater and airflow motor. Consequently, the heating time was fixed at 30 s, with the inlet airflow speed set to 15 m/s and wind pressure set to 145 N/m^2 to optimize airflow temperature, as shown in Figure 7.

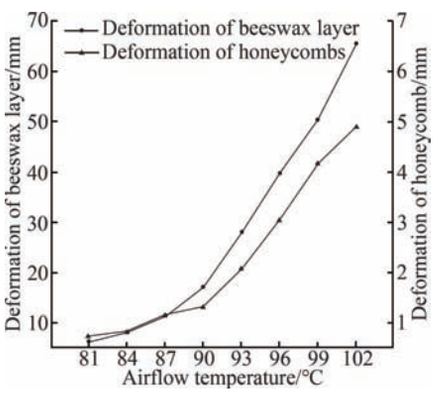


Figure 7　Numerical simulation of variation of average total deformation with temperature

Numerical data demonstrated that the beeswax layer had already begun to melt effectively at 81 ℃. Prior to reaching 87 ℃, the deformation disparity between the two was relatively small, and the influence of temperature variations on deformation was not pronounced. However, subsequent to 87 ℃, the deformation disparity between them gradually widened. After 96 ℃, the melting of the beeswax layer was nearly complete. However, the total deformation of the honeycombs continued to increase at a relatively high rate. Therefore, 90 ℃ was chosen as the optimal melting temperature. Then, the inlet temperature was set to 90 ℃ and the airflow speed was adjusted. Figure 8 shows the impact of airflow speed on the deformation of both the beeswax layer and honeycombs.

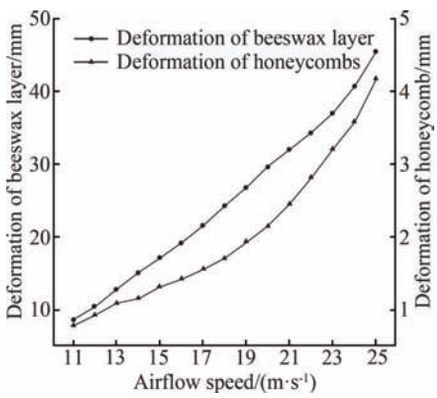
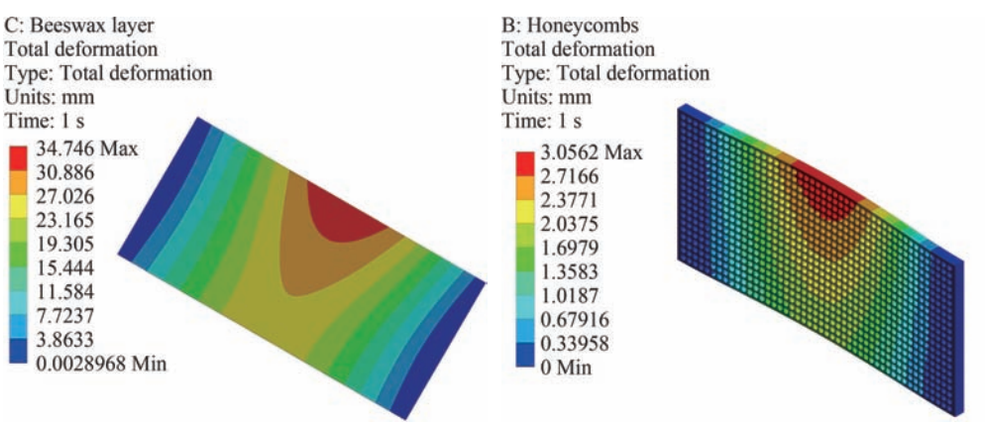


Figure 8　Numerical simulation of variation of average total deformation with airflow speed

Numerical data demonstrated that the disparity in deformation between the honeycombs and the beeswax layer progressively increases in the airflow speed range of 11 to 20 m/s. When the airflow speed exceeds 19 m/s, the deformation approaches the upper limit for the honeycomb's structural integrity. Consequently, the median speed of 15 m/s, within the range of 11 to 19 m/s, was determined to be the optimal airflow speed for the operation of the beeswax layer-melting apparatus. The deformation of the honeycombs and beeswax layer at the optimal melting temperature of 90 ℃ and the optimal airflow speed of 15 m/s are shown in Figure 9.



(a) The deformation of beeswax layer　　(b) The deformation of honeycombs

Figure 9　Deformation of honeycombs and beeswax layer at 90 ℃ and 15 m/s airflow speed

The damage of honeycomb materials was caused by the combined processes of thermal convection and wind pressure. When comparing the impact of temperature and airflow speed variations on the

deformation of the honeycombs and beeswax layer, temperature exerted a greater influence. This could potentially be attributed to the proximity of the air outlet to the honeycomb, facilitating efficient heat transfer.

2.2 Field experiments

This study conducted experiments to verify the stability of the overall structure of the automated honey-harvesting robot, as well as the practical performance of the beeswax-melting device was also assessed. The experiments encompassed a range of operational procedures, including the operation of beehive covers and beehive frames, melting of beeswax, and transportation of these frames to a centrifuge, as shown in Figure 10. Each procedure was replicated ten times to ensure the reliability of the results. The duration of each experiment was timed, the success rate of extracting beehive frames from the beehives and feeding them into the centrifuge was also recorded. Additionally, the degree of beeswax layer-melting and honeycomb damage were documented. The degree of honeycomb damage and beeswax layer melting were approximately determined by measuring the affected areas before and after the experiment, and the results were rounded down. All these results are presented in Table 3.



(a) Extraction of the beehive frames (b) Transportation of the beehive frames (c) Beehive frames fed into centrifuge

Figure 10 The process of field experiments for automated honey-harvesting robot

Table 3 The result of field experiments

Number of beehive frames	Experiment duration/s	Success rate of the handling of beehive frames/%	Degree of honeycomb damage/%	Degree of beeswax layer melting/%
1	98	98.6	26	80
2	197	98.6	28	83
3	300	98.6	27	85
4	413	92.8	26	86
5	527	91.4	25	84
6	636	90.0	27	82
7	743	88.6	28	85

The experimental results indicated that the automated honey-harvesting robot could complete a significant portion of the honey extraction process with notable efficiency. Instances of improper beehive frame manipulation during the experiment may be attributed to relative displacement between the frames and the beehive frame handling device, which was caused by road-borne vibrations. This displacement led to misalignment during frame placement in the centrifuge. Furthermore, the optimized beeswax layer-melting apparatus exhibited consistent performance in liquefying the beeswax layer, while preserving the structural integrity of the honeycombs to a considerable extent. However, the degree of honeycomb's damage remains relatively high, likely attributed to the air pressure of the beeswax layer-melting apparatus was maintained at a constant value throughout the melting process, thereby failing to dynamically adapt to the evolving thermal and physical properties of the beeswax layer as it underwent liquefaction.

3 Conclusion

This study presents the design of an automated honey-harvesting robot developed to avoid direct human-bee interaction, thereby reducing beekeepers sting risk. The robot's functionalities encompass

autonomous navigation, identification of beehives, automatic operation of the beehive covers and beehive frames, and automatic beeswax layer-melting. Moreover, the beeswax layer-melting apparatus designed in this study employs a controlled thermal process for the removal of beeswax layer, which minimizes the damage to the honeycombs compared to manual methods and provided an even purer material for the subsequent centrifugal honey extraction process. The feasibility of the automated honey-harvesting robot was validated through field experiments.

Key design parameters were rigorously determined. The minimum suction force for the beehive frame handling device was determined to be 47.7 N. The standard pixel count, utilized for comparison purposes to adjust the robot pose, was determined to be 1.62×10^5 pixels. Based on the fluid-structure interaction method utilizing FLUENT/Mechanical, this study conducted numerical simulations on the beeswax layer-melting in honeycombs to optimize its working parameters. The heating time was preset at 30 s, and through subsequent simulation experiments, the optimal airflow velocity and temperature of the beeswax layer-melting apparatus were determined to be 15 m/s and 90 ℃ respectively. It could achieve effective melting of the beeswax layer while maintaining minimal damage to the honeycombs (less than 30%).

The automated honey-harvesting robot showed promising applications in the beekeeping industry. Future development will focus on monitoring and real-time control of the beeswax layer-melting apparatus operational process to minimize honeycomb damage further. In addition, Integration of a compact centrifugal module on the robot is planned to combine the two processes of honey harvesting and purification into a single, thereby enhancing work efficiency. Continuous optimization will strive to achieve work efficiency comparable to that of human labor. By integrating honey-harvesting robots with advanced recognition algorithms, Internet of Things devices and standardized apiary systems, more intelligent honey harvesting operations could be achieved.

References

[1] EL-DIDAMONY S E, GOUDA H I A, ZIDAN M M M, et al. Bee products: An overview of sources, biological activities and advanced approaches used in apitherapy application [J]. Biotechnology Reports, 2024: e00862.

[2] WANG Q, GAO H X, CHEN D H, et al. Analysis on the distribution characteristics of honey production in China [J]. Special Wild Economic Animal and Plant Research, 2023, 45(6): 166−172.

[3] LI Q F, WANG X J, CHEN M, et al. Comparative study on quality standards of honey at home and abroad [J]. Journal of Zhejiang Agricultural Sciences, 2024, 65(1): 8−15.

[4] PHIRI B J, FèVRE D, HIDANO A. Uptrend in global managed honey bee colonies and production based on a six-decade viewpoint, 1961-2017 [J]. Scientific Reports, 2022, 12(1): 21298.

[5] GAO Y, LIU J, ZHAO Z J, et al. Analysis on global honey trade and its future prospects [J]. Agricultural Outlook, 2022, 18(5): 112−117.

[6] SGROI F, MODICA F. An experimental analysis of consumers′ attitudes towards honey: The case of the Sicilian market [J]. Future Foods, 2023, 7: 100223.

[7] KAUR B, DIMRI S, SINGH J, et al. Insights into the harvesting tools and equipment′s for horticultural crops: From then to now [J]. Journal of Agriculture and Food Research, 2023, 14: 100814.

[8] WANG P, KIM S, HAN X. Development of an automatic beehive transporting system based on YOLO and DeepSORT algorithms [J]. Computers and Electronics in Agriculture, 2025, 229: 109749.

[9] WANG Z Y, DU Y X, LI J J, et al. Changes in health-promoting metabolites associated with high-altitude adaptation in honey [J]. Food Chemistry, 2024, 449: 139246.

[10] LUO X, DONG Y, GU C, et al. Processing technologies for bee products: An overview of recent developments and perspectives [J]. Frontiers in Nutrition, 2021, 8: 727181.

[11] CARON D S A A D M. The Beekeeper′s handbook [M]. Comstock Publishing Associates, 2021.

[12] BAGLIO E, BAGLIO E. Honey: Processing techniques and treatments [J]. Chemistry and Technology of Honey Production, 2018: 15−22.

[13] BABARINDE G O, BABARINDE S A, ADEGBOLA D O, et al. Effects of harvesting methods on physicochemical and microbial qualities of honey [J]. Journal of Food Science and Technology, 2011, 48: 628−634.

[14] MUTHUSAMY S K, SANGEETHA S V T, AL BUSAIDI A S, et al. Design and development of drone based remote controlled honey harvesting machine [C]// 2021 Fifth International Conference on I-SMAC (IoT in Social, Mobile, Analytics and Cloud)(I-SMAC). IEEE, 2021: 1212−1217.

[15] BAC C W, VAN HENTEN E J, HEMMING J, et al. Harvesting robots for high-value crops: State-of-the-art review and challenges ahead [J]. Journal of Field Robotics, 2014, 31(6): 888－911.
[16] LIU C L, GONG L, YUAN J, et al. Current status and development trends of agricultural robots [J]. Transactions of the Chinese Society for Agricultural Machinery, 2022, 53(7): 1－22, 55.
[17] KASTRATOVIĆ V. Some aspects of beeswax hydrolysis [J]. Agriculture and Forestry, 2022, 68(4): 79－88.
[18] BOGDANOV S. Beeswax: Production, properties, composition, control [J]. Bee Product Science, 2016.
[19] HOU G, WANG J, LAYTON A. Numerical methods for fluid-structure interaction －A review [J]. Communications in Computational Physics, 2012, 12(2): 337－77.
[20] GAO S Z, WANG Y J, ZHANG Y M, et al. Simulation analysis of frictional heat and temperature field of deep groove ball bearings [J]. Machinery Design & Manufacture 2024: 1－5.
[21] ZHANG H, LIU Y B, KONG L H, et al. A study on reproductive and wax-moth defense abilities of honeybees (apis cerana cerana) in multiple-layer hives [J]. Acta Agriculturae Universitatis Jiangxiensis, 2020, 42 (1): 157－163.
[22] VOIKU I P. Trends and prospects of technical support for separating beehive frames from the hive body [C]// IOP Conference Series: Earth and Environmental Science. IOP Publishing, 2021, 839(5): 052049.
[23] HE F P, ZHANG Z, MA Z G. Review on the reasonable selection of beehive and matters needing attention [J]. Journal of Bee, 2021, 41(10): 4－8.
[24] DAI S T, WANG Y SHANG C C. Multi-unmanned vehicle collaborative path planning method based on deep reinforcement learning [J/OL]. Journal of Beijing University of Aeronautics and Astronautics, 2024: 1－12 [2025－03－03].
[25] XIAO Y, ZHOU J. Overview of image edge detection [J]. Computer Engineering and Applications, 2023, 59 (5): 40－54.
[26] CHEN Guiyun, WU Wei, CHEN Kunjie. Effects of temperature, moisture content and adulterationon honey viscosity [J]. Journal of Nanjing Agricultural University, 2008, 211(1): 121－127.
[27] TIMBERS G E, GOCHNAUER T A. Note on the thermal conductivity of beeswax [J]. Journal of Apicultural Research, 1982, 21(4): 232－235.
[28] LI Guichuan, LI Haiyu, YANG Shaopeng, et al. Simulation and experiment of distributors of different outlet types of pneumatic collection and discharging systems based on CFD-DEM coupling [J]. Journal of Intelligent Agricultural Mechanization, 2024, 5(1): 1－11..
[29] BUCHWALD R , BREED M D , GREENBERG A R . The thermal properties of beeswaxes: Unexpected findings [J]. Journal of Experimental Biology, 2008, 211(1): 121－127.

蜂蜜自动化采收机器人的设计与试验

张迪[1]，王春颖[1, 2, 3]，杨明国[1]，孙梓轩[1]，刘平[1, 2, 3*]

（1. 山东农业大学机械与电子工程学院，山东泰安，271000；2. 农业装备智能化山东省工程研究中心，山东泰安，271000；3. 山东省设施园艺智慧生产技术装备重点实验室（筹），山东泰安，271000）

摘要：当前，蜂蜜生产主要依赖于个体养殖模式，规模小且分布零散。传统的蜂蜜采收涉及人工提取巢框，切割蜜蜡层和离心取蜜。这一过程不仅劳动强度大，还存在养蜂人被蜜蜂蜇伤的风险。此外，人工割蜡技术往往会导致蜜脾结构受损，且蜜蜡层去除效果不彻底。本研究设计一款蜂蜜自动化采收机器人，旨在避免人—蜂接触，实现巢框提取、蜡层去除等自动化蜂蜜采收作业。该机器人主要由行走装置、巢框操作装置、工业相机、蜡层熔化装置和控制器组成。基于图像识别技术实现蜂箱识别，控制器控制行走装置行进到蜂箱位置，并通过比较像素点进行行走装置位姿调矫正。设计基于磁力吸附的巢框操作装置，巢框操作装置最大吸力达到60.8 N，电磁铁通断电与十字滑台结合，实现蜂箱盖的开合与巢框的取放作业。为实现蜜蜡层温和去除，设计了蜡层熔化装置。热流实验首先确定其有效参数范围，进而在预设的30 s加热时间下，通过FLUENT/Mechanical流－固耦合仿真确定15 m/s的最佳气流速度和90 ℃的最佳熔化温度。田间试验结果：巢框的取放成功率高于85%，蜜蜡层熔化程度高于80%，且熔化后蜜脾的损伤程度低于30%。试验结果表明，蜜蜂自动化采收机器人整体结构可靠，可自动化完成巢框取放、蜜蜡层熔化等蜂蜜采收作业，蜡层熔化装置在最优参数设置下能有效熔化蜜蜡层，同时对蜜脾的损伤程度较低。本研究减轻了蜂农的劳动强度，有效避免了人—蜂接触的风险，而且改善了蜜蜡层的去除效果，对推动现代蜂业的进步具有重要指导意义。

关键词：蜂蜜采收；自动化；蜜蜡层熔化；流—固耦合；参数优化